

Mechanical properties of axially loaded threaded rods after dis- and reassembly

Alisa Resch¹, Haris Stamatopoulos²

ABSTRACT: This pilot study investigates the mechanical properties of axially loaded threaded rods, screwed-into spruce glulam elements, both parallel and perpendicular to the grain. The effect of disassembly and reassembly was quantified through experimental tests on rods that were unscrewed and rescrewed into the same glulam elements. Withdrawal stiffness was determined under service-level cyclic loading before and after reassembly. Additionally, the capacity and failure modes of all specimens were identified through monotonic tensile loading until failure and compared to reference tests. A decrease in stiffness was observed across all loading conditions between the first and second assembly. After reassembly, the remaining monotonic stiffness under tension loading was 73 % for rods embedded perpendicular to the grain and 80 % for rods embedded parallel to the grain. In compression loading, both orientations exhibit a smaller reduction, retaining 85 % of their original monotonic stiffness. The most significant drop occurred in fully reversed cyclic loading due to increased pinching effects. Despite this reduction in stiffness, the rods maintained relatively high overall stiffness. Furthermore, reassembly showed no impact on capacity for rods perpendicular to the grain. For rods parallel to the grain a small decrease in capacity was observed but it could not be concluded whether this was a result of rescrewing or the natural variability of the material. The ease of dis- and reassembly and the obtained mechanical properties indicate the suitability of reassembled rods in high-performance timber connections.

KEYWORDS: Threaded rods, withdrawal, glulam, dis- and reassembly, reuse

1 – INTRODUCTION

The construction industry is a main contributor to greenhouse gas emissions (GHG), the waste stream and consumption of primary resources. The concept of circular economy is one strategy to reduce emissions and increase efficient use of material resources. According to the waste hierarchy, concepts of “Reduce” and “Reuse” are preferred over what is common practise right now (“Landfill”, “Inclination”, “Recycle”). By extending the lifespan of materials and elements to a maximum, the overall environmental performance of buildings can be improved significantly. Especially structural elements carry big potential if (re-)used at their highest quality, instead of downgrading them (e.g. structural timber to particle boards). However, structural safety is depending on the mechanical properties of elements, connections and materials in the building. When maximizing the lifespan of elements by reusing them in multiple life cycles, the knowledge on their alternated properties is vital to ensure both structural safety and a material-efficient design. In multi-storey timber buildings, the

mechanical properties of the connections are of major importance for the overall structural performance. In comparison to steel and concrete, timber is a lightweight and environmental friendly building material. However, the weight-to-strength ratio bears some challenges when it comes to wind-induced vibrations and deflections. To achieve sufficient serviceability limit state requirements in high-rise timber buildings, high performance and stiff connections are vital. Long spans and the separation of the load-bearing frame to create flexible and adaptable rooms is one frequently mentioned design strategie in literature to facilitate a possible reuse of elements at the end of life (EoL). Another recurring aspect is a simple design with the same standardised components and connections and generally reduced complexity. To achieve a proper design for disassembly (DfD), joints need to be accessible, reversible, easily dismantable and well documented. In comparison to glued connections, screws, bolts, and dowels are ranked as (mostly) suitable for reversible connections in a guide on reuse of structural elements by Hradil et al. [1]. However, it is stated that “*the same connector is not as effective in the*

¹ Alisa Resch, NTNU, Trondheim, Norway, alisa.t.resch@ntnu.no

² Haris Stamatopoulos, NTNU, Trondheim, Norway, haris.stamatopoulos@ntnu.no

same hole". Most research on reuse focuses on the structural level with the aim to keep the timber elements at the biggest size and the highest quality as possible. Even though the connections are a key element to achieve this goal, at a joint level, the fasteners are mostly considered for recycling. A review by Ottenhaus et al. [2] on reversible timber connection systems identifies the performance after repeated dis- and reassembly and the effect of reversed cyclic loading as one challenge that needs to be addressed in further research.

Connections with axially loaded threaded rods feature a high stiffness and capacity. Due to the ease of the screwing process, they can be both preinstalled and easily dismantled, offering a big potential for reuse of structural timber components. Former research has been mostly done on self-tapping screws (STS) with a smaller diameter or glued-in rods with similar dimensions. Binck and Frangi [3] carried out a study on the withdrawal properties of both glued-in and threaded rods parallel to the grain. At NTNU, various experiments on the mechanical properties of axially loaded, screwed-in threaded rods have been carried out [4], [5], [6], [7]. One possible application is in a column-to-beam connection to create moment-resisting frames with long spans and a certain level of ductility and tolerances as described in [8]. Although the properties of screws and threaded rods have been extensively investigated, very little is known about their mechanical properties after dis- and reassembly (i.e. unscrewing and rescrewing). In this paper, the effect of dis- and reassembling of axially loaded threaded rods is evaluated based on cyclic, service-level testing and monotonic destructive testing.

2 – PROJECT DESCRIPTION

In this study, glulam specimens with axially loaded threaded rods were tested in a pull-push configuration. The glulam is made from Norwegian spruce (*picea abies*) of strength class GL30c, according to EN14080:2013 [9] and the dimensions of the specimens were 550 mm × 450 mm × 140 mm. The specimens were predrilled with the core diameter d_i before screwing-in the rods perpendicular ($\alpha = 90^\circ$) or parallel to the grain ($\alpha = 0^\circ$). In the opinion of the authors, rods inserted parallel to the grain should be avoided in practice due to the risk of splitting. However, tests with rods parallel to the grain, i.e. in the material axis can provide material characterization and valuable information for small angles. Purpose-made threaded rods of strength grade 8.8 were used in the tests, see *Figure 1*. The rods consist of a 22 mm outer-thread diameter (d) and a 16.1 mm core diameter (d_i). The embedment length of the woodscrew thread was 440 mm. In their end, the rods have a 110 mm

long metric thread which allows them to connect with other parts. The geometry of the threaded rod is displayed in *Figure 1*.



Figure 1. Geometry of the threaded rod

All specimens were first tested in service-level, cyclic loading up to approximately 40 % of their estimated capacity. The capacity of $F_{ax,est} = 120$ kN was calculated according to (1) from former experiments at NTNU by Stamatopoulos and Malo [5] on rods with 20 mm outer-thread diameter.

$$F_{ax,est} \approx 15 \cdot d \cdot l \cdot \frac{\rho_{mean}}{470} \quad (1)$$

All cyclic tests were performed in tension (12 kN to 48 kN), compression (-12 kN to -48 kN) and fully reversed (-48 kN to 48 kN) loading with 8 full cycles for each mode. *Figure 2* shows examples of load-displacement curves under cyclic loading that include two different stiffness estimates $K_{ax,cyc}$ and $K_{ax,mon}$. The top graph depicts a typical hysteresis loop under unidirectional loading (tension or compression), demonstrated by an exemplary tensile loading protocol. The bottom graph illustrates a typical hysteresis loop under fully reversed loading, where the rod is exposed to alternating loading in both directions.

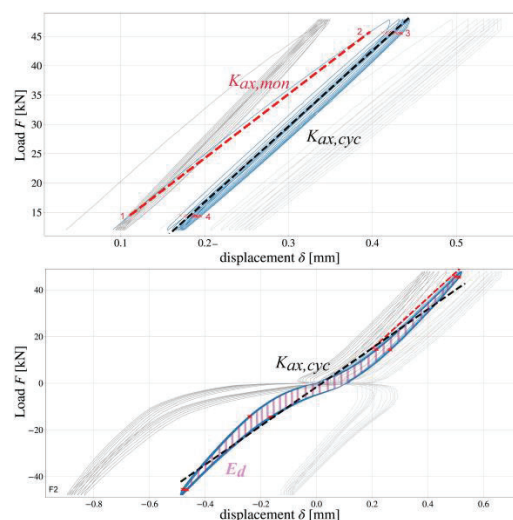


Figure 2: Load-displacement curves in tension loading (top) and fully reversed loading (bottom)

Table 1: Experimentally recorded withdrawal stiffness K_{ax} and capacity F_{ax} for splitting (s) and withdrawal (w) of different assembly groups

Group	n	Assembly	Withdrawal stiffness K_{ax} [kN/mm]				Capacity F_{ax} in [kN]			
				$\alpha = 90^\circ$		$\alpha = 0^\circ$		$\alpha = 90^\circ$	$\alpha = 0^\circ$	
1	6+6	1. gradually	$K_{ax,mon,T}$	116.6		196.5		157.4 (w)	126.3 (w)	137.2 (s)
2	6+6	1. completely	$K_{ax,mon,T}$	141.2		184.3				
			$K_{ax,mon,C}$	87.1		140.6				
			$K_{ax,eye,T}$	180.5		234.7				
			$K_{ax,eye,C}$	106.6		188.2				
			$K_{ax,eye,FR}$	113.2		145.6				
		2. completely	$K_{ax,mon,T}$	103.5	↓ 27%	147.8	↓ 20%	159.6 (w)	101.5 (w)	120.3 (s)
			$K_{ax,mon,C}$	73.4	↓ 16%	119.6	↓ 15%			
			$K_{ax,eye,T}$	143.8	↓ 20%	209.5	↓ 11%			
			$K_{ax,eye,C}$	98.2	↓ 8%	176.6	↓ 6%			
			$K_{ax,eye,FR}$	69.1	↓ 39%	113.9	↓ 22%			
3 (ref)	3+3	1. completely	$K_{ax,mon,T}$	109.1		164.1		145.0 (w)	122.6 (w)	133.3 (s)

The main aim of this study is to analyse the influence of screwing and unscrewing on the mechanical properties of the threaded rods regarding possible reassembling. Therefore three different groups were tested, which are also displayed in Table 1.

- **Group 1** consists of 12 specimens (6 with rods inserted parallel to the grain and 6 with rods inserted perpendicular to the grain). In this group, the rods were screwed-in gradually at embedment lengths 110, 220, 330, 440 mm and tested non-destructively at each length. In the end, the rods were tested destructively for the final embedment length of 440 mm.
- **Group 2** consists of 12 specimens (6 with rods inserted parallel to the grain and 6 with rods inserted perpendicular to the grain). In this group, the specimens were tested initially non-destructively at an embedment length of 440 mm followed by unscrewing and rescrewing of the rods and repeat of the tests. The purpose of this process was to simulate a scenario where the rods are disassembled after a given amount of time in a building and reassembled. Assuming the standard buildings' lifespan of 50 years, it is very likely that rods will be exposed to higher levels than service-level loading due to higher loads in their service life. Therefore group 2 was exposed to an additional monotonic load in tension and compression prior to disassembly. This load was determined to 100 kN for perpendicular and 75 kN for parallel to the grain rods. These forces are deemed close to the design resistance values of the rods. The load levels are based on the characteristic withdrawal capacity $F_{k,exp}$ which was obtained out of the destructive testing in

group 1. To obtain approximate design values, the characteristic withdrawal capacity was divided by a safety factor of $\gamma_m = 1.3$. This was an oversimplified procedure to take into account the fact that rods will experience greater forces during the service life than the the service-level ones. The sequence of higher loads in structures can vary widely over their lifetime and together with climatic conditions this may have an effect, but this effect is outside the scope of the present study. In the end, the rods were tested destructively.

- **Group 3** is a reference group where the rods were inserted and tested directly at an embedment length of 440 mm; first in non-destructive cyclic loading and then destructively.

The specimens in all groups were tested destructively in monotonic tension according to EN26891 [11]. The tests carried out for each group are summarized as follows :

- Cyclic loading in service-level to +/- 48 kN
→ group 1,2,3
- Monotonic loading to +/- 100 kN ($\alpha = 90^\circ$) or +/- 75 kN ($\alpha = 0^\circ$)
→ group 2
- Monotonic tension until failure
→ group 1,2,3

3 – EXPERIMENTAL SETUP

Figure 3 shows the setup of the tests pull-push configuration. Prior to testing, all specimens were stored in standard temperature and relative humidity conditions (20 °C / 65% RH). The average moisture content was

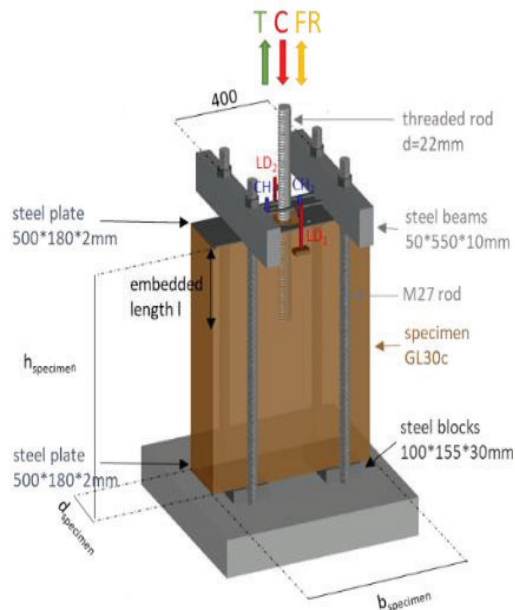


Figure 3: Experimental setup in cyclic, service-level loading

checked on different faces of each specimen and found in the expected range of 10 - 12 %. The load was applied to the top of the rods in their metric threaded end (at $l_0 = 100$ mm). The specimens were firstly tested non-destructively in tensile, compressive and fully reversed cyclic loading, as specified in Section 2. Displacement measurements were taken with four linear variable displacement transducers (LVDT) placed either on the side or on top of the specimen to calculate the axial stiffness. They result in two different average values of two opposing LVDTs respectively, The measurements on the sides (LD) were used as the main displacement measurement in this work. All LVDTs were attached to the rod with a metal cross, 50 mm above the entrance point of the rod as shown in Figure 4. The axial stiffness in service-level loading K_{ax} was back-calculated from the experimental data (K_{exp}) and the free length of $l_0 = 50$ mm (K_{l_0}) as springs in series with the following equation (2).

$$K_{ax} = \frac{K_{exp} \cdot K_{l_0}}{K_{l_0} - K_{exp}} \quad (2)$$

In the final round, destructive monotonic tensile loading according to EN 26891 [11] was applied and the withdrawal capacity and failure modes were identified. Two steel plates were installed at the top and bottom, to distribute the forces more evenly and reduce opening stresses in the specimens with parallel to the grain embedded rods. The process includes predrilling the

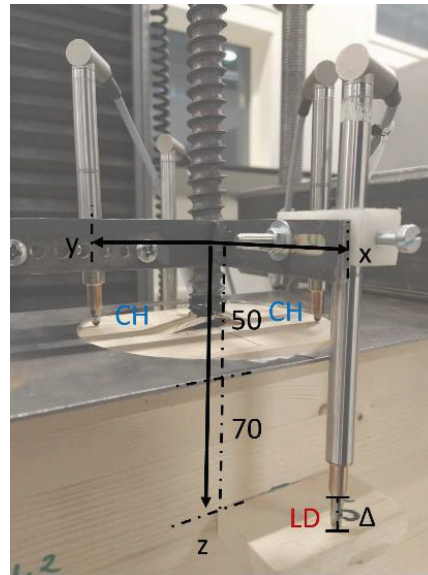


Figure 4: Displacement measurements with LVDTs on top (CH) and on the side (LD)

holes, screwing the rods, attaching and placing the LVDTs and connecting the machine. The process was fairly simple and involved standard tools. There was no noticeable difficulty in un- and rescwinging of the rods, showing great potential for easy and fast assembly and disassembly of threaded rods without causing damage.

4 – RESULTS

The experimental data was analysed with a python script, using the mean displacement between two opposing LVDTs for the calculations (LD). The arrangement of the LVDTs on opposing sides of both axes is essential in order to obtain an accurate mean value that is not affected by potential rigid-body rotation of the specimen. When looking at the individual values, it becomes apparent that one LVDT alone would not be sufficient. This is illustrated in Figure 2, with the individual LD measurements plotted in grey in the background and the mean curve shown in blue. Therefore, only average values from clean measurements on both sides were used.

4.1 – MEASURING METHOD

The method of measurement and the placement of the LVDTs had an impact on the results. When comparing the individual stiffness measurements for each test specimen, slight variations were observed between the LD and CH measurements. This difference was most noticeable for rods embedded parallel to the grain with deviations of up to 17 %. Despite these variations, the mean values obtained for both measurement points were similar.

4.2 – STIFFNESS OF REASSEMBLED RODS

Figure 5 illustrates the monotonic axial stiffness measurements taken after the first and second rounds of assembly for all individual specimens. The measurements are shown for both tension (left) and compression (right) loading.

For the initial assembly, the monotonic axial stiffness of the rods embedded perpendicular to the grain ranged from 124.3 kN/mm to 161.8 kN/mm in tension and 81.7 kN/mm to 98.1 kN/mm in compression. This results in a mean stiffness of 141.2 kN/mm (CV = 9.2 %) in tension and 87.1 kN/mm (CV = 6.9 %) in compression. As shown in Figure 5, after reassembly, the stiffness consistently decreased compared to the first assembly. The average monotonic axial stiffness of the rods embedded perpendicular to the grain decreased from 141.2 kN/mm to 103.5 kN/mm in tension, leading to a remaining monotonic stiffness of 73 % after reassembly. For the parallel to the grain embedded rods, the remaining stiffness was approximately 80 %, with a decrease from 184.3 kN/mm to 147.8 kN/mm. In compression, both angles to the grain ($\alpha = 0^\circ$ and

$\alpha = 90^\circ$) exhibited a similar remaining stiffness after reassembly of 85 %. The monotonic axial stiffness in compression decreased from 87.1 kN/mm to 73.4 kN/mm for the perpendicular to the grain embedded rods and from 140.6 kN/mm to 119.6 kN/mm for the parallel embedded rods.

The decrease in stiffness could be related either to the wood component, the screwing of the threaded rod or a combination of both. The rescrowing and loading presumably leads to micro-fractures and some material damage in the wood around the thread, allowing the rod to move more freely and therefore reducing the overall stiffness. Why this effect seems more prominent in tension than in compression is not clear to the authors. Another possible explanation could be that in the process of rescrowing, it is not certain that the rod will follow exactly the same path as the first time. These observations are fundamental to understanding the practical implications of reusing threaded rods in a structure. As mentioned by Hradil et al. [1] “the same connector is not as effective in the same hole”.

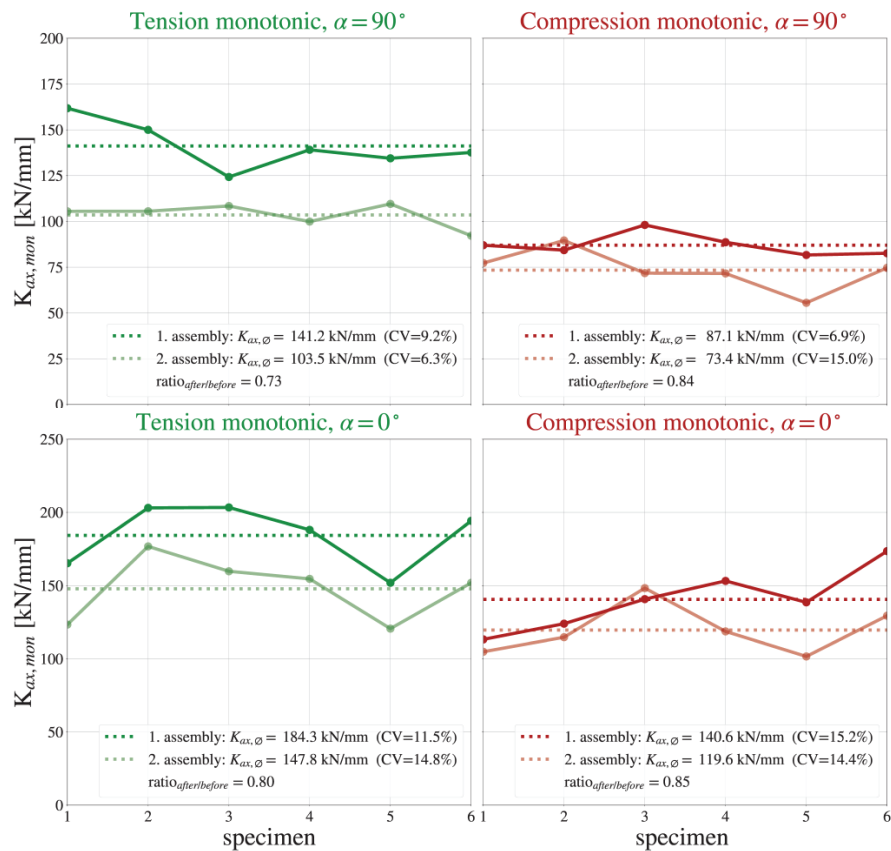


Figure 5: Monotonic axial stiffness after 1st and 2nd assembly in tension and compression service-level loading

4.3 – TENSION VS COMPRESSION

The monotonic axial stiffness in compression was found to be lower than in tension. For the perpendicular to the grain embedded rods, the mean monotonic axial stiffness in compression was determined to be 87.1 kN/mm. This is a reduction of 39 % compared to the corresponding stiffness of 141.2 kN/mm under tension loading. For the rods embedded parallel to the grain, the mean monotonic axial stiffness in compression was determined to be 140.6 kN/mm which is 24 % lower than the observed 184.3 kN/mm in tension.

4.4 – ANGLE TO THE GRAIN

Parallel to the grain embedded rods exhibit a 30 % higher monotonic axial stiffness than the perpendicular to the grain ones in tension loading. In compression the monotonic axial stiffness is even 61% higher. However, this higher stiffness also comes with a greater variability between individual measurements, indicated by higher coefficients of variation (*CV*) for parallel to the grain embedded rods in comparison with the perpendicular embedded ones. This variability can be attributed to the number of laminations the rod penetrates. Since parallel to the grain embedded rods pass through only a single lamination, the homogenization effect is absent, making axial stiffness and other mechanical properties more variable at smaller angles to the grain (α). In this study, only the limiting cases of $\alpha = 0^\circ$ and $\alpha = 90^\circ$ were analyzed, establishing a stiffness range between 140 kN/mm and 185 kN/mm. The axial stiffness for intermediate angles is expected to fall within this range.

4.5– CYCLIC STIFFNESS

Under service-level cyclic loading, two types of axial stiffness were determined from each dataset. The first one is the immediate stiffness after the initial load uptake in the first cycle, denoted as monotonic axial stiffness $K_{ax,mon}$. Additionally, a cyclic axial stiffness $K_{ax,cyc}$ was calculated as a linear fit across all subsequent cycles (2-8). The determination of these different stiffnesses is illustrated in the load-displacement curves in *Figure 2*. The individual and mean cyclic stiffnesses for the loading conditions tension, compression and fully reversed are illustrated in *Figure 6*, both before and after reassembly. A comparison of $K_{ax,cyc}$ with $K_{ax,mon}$ revealed the following key observations:

Rods with $\alpha = 90^\circ$:

- $K_{ax,cyc}$ is generally higher than $K_{ax,mon}$
- The differences of $K_{ax,cyc}$ in between first and second assembly are less prominent than for the monotonic axial stiffness $K_{ax,mon}$ in tension and compression loading.
- In fully reversed loading, the decrease in mean cyclic axial stiffness $K_{ax,cyc}$ between first and second assembly is notably high. The remaining cyclic stiffness after reassembly is 61 %. Presumably, the combined effects of both tension and compression contribute to this reduction. As the load reverses around 0 kN, the damaged wood experiences its greatest impact in both directions. The rod repeatedly passes through its loosest position, leading to a pinching effect and reduction in stiffness. This pinching effect is evident in the direct comparison of the hysteresis loops between the first and second assembly displayed in *Figure 7*.

Rods with $\alpha = 0^\circ$:

- $K_{ax,cyc}$ is generally higher than $K_{ax,mon}$
- The differences of $K_{ax,cyc}$ between first and second assembly are less prominent than for the monotonic axial stiffness $K_{ax,mon}$ in tension and compression loading.
- In fully reversed loading, the decrease in stiffness between first and second assembly is the highest, as the damaging effects on the wood accumulate in both directions. After reassembly, 78 % of the cyclic stiffness remains, which is still significantly higher than the 61 % retention observed for rods embedded perpendicular to the grain. This suggests that rods cause greater damage when rescrewed perpendicular to the fibers. As perpendicular to the grain direction is generally less stiff, the rod may follow a slightly different path during the second assembly, creating larger gaps and damage in the immediate interface. Conversely, when rods are screwed parallel to the grain, the material is much stiffer, and the rod is more likely to follow its original path, aligning with the fibre direction. As the thread presumably retraces the same path during reassembly, less damage occurs, leading to a smaller reduction in stiffness.

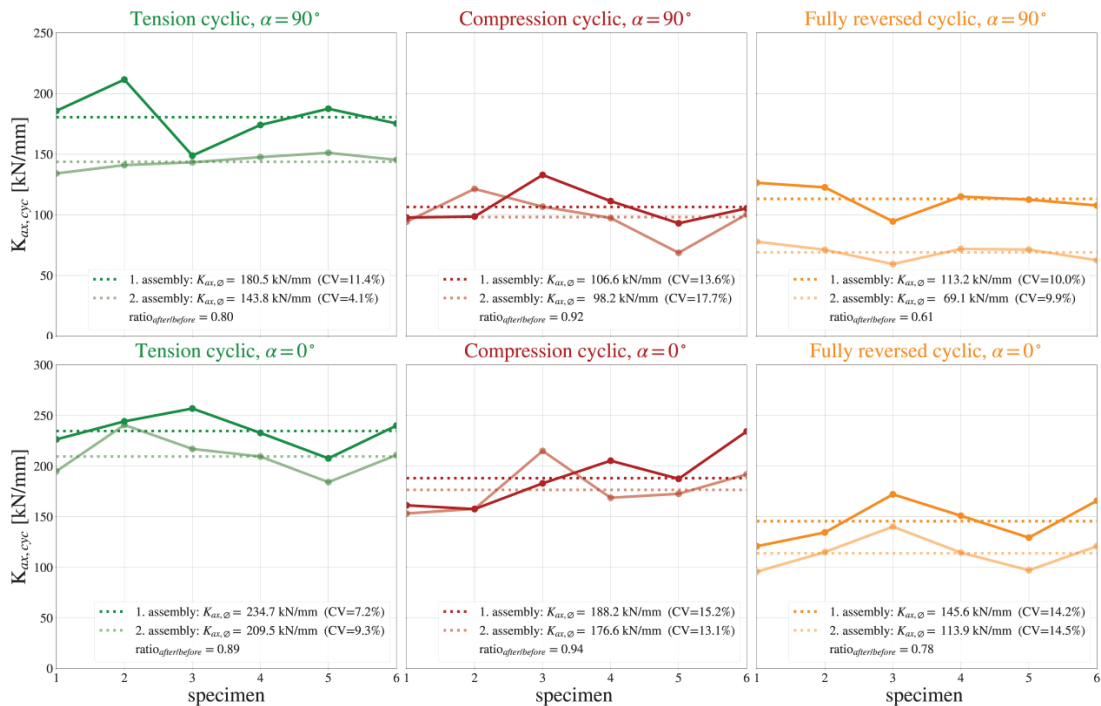


Figure 6: Cyclic axial stiffness after 1st and 2nd assembly in tension, compression and fully reversed service-level loading

4.6 – EQUIVALENT VISCOUS DAMPING

The equivalent viscous damping ratio ξ_{eq} is a non-dimensional parameter which provides a representation of the dissipated energy E_d at service-level loading. It was calculated with eq. (3) out of the cyclic stiffness K_{cyc} and the loading amplitude F_a illustrated in the hysteresis loops of Figure 2.

$$\xi_{eq} = \frac{1}{2\pi} \frac{E_d * K_{cyc}}{F_a^2} \quad F_a = \frac{F_{max} - F_{min}}{2} \quad (3)$$

Eq.(3) is obtained on a similar basis as in EN12512 [12]. In this test series, damping ratios between 0.02 and 0.05 were found. This is in agreement with former studies on threaded rods in CLT [4]. There was no significant effect on the damping ratio due to reassembly.

4.7– REFERENCE GROUPS

The stiffness values can be better understood in comparison with the reference groups. Table 1 provides the monotonic axial stiffness and capacity for all three groups for the perpendicular and parallel to the grain embedded rods. The values of group 1 and 3 were generally in good agreement with each other. Notably, the axial stiffness of the 90° rods is significantly higher

than the reference groups 1 and 3. This could be due to small differences in the setup or positioning of the LVDTs or the inherent material variability. However, the conclusion about the effect of dis- and reassembly remains valid, even if the absolute mean values may differ between the groups, as in group 2 the same specimens were tested in two rounds.

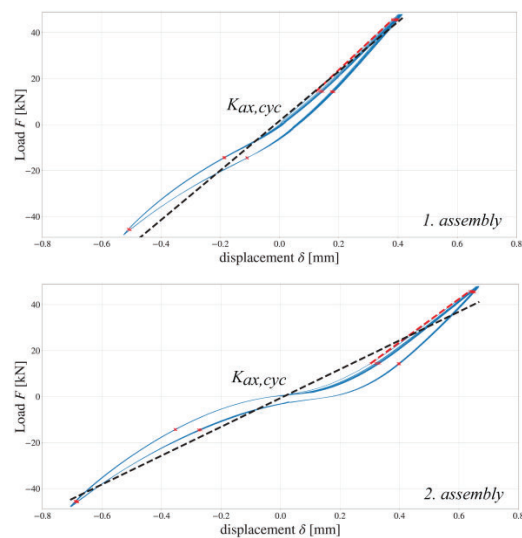


Figure 7: Load-displacement curve in fully reversed loading after the 1st assembly (top) and 2nd assembly (bottom) for $\alpha=90^\circ$

Comparing groups 1 and 3, the gradual screwing of the rods in group 1 did not show any significant deviations

4.8– FAILURE MODES AND CAPACITY

Figure 8 and Figure 9 illustrate the final destructive tension loading of all specimens. The individual results of the rods with $\alpha = 90^\circ$ of group 2 are plotted in fainter colours in the background with the mean curves of each group respectively. It is noticeable that mean withdrawal capacity $F_{ax,90^\circ}$ of group 2 is with 159.0 kN the highest in comparison with group 1 and 2.

- Group 1: $F_{ax,90^\circ} = 157.1 \text{ kN}$ (CV = 4.7 %)
- Group 2: $F_{ax,90^\circ} = 159.0 \text{ kN}$ (CV = 4.2%)
- Group 3: $F_{ax,90^\circ} = 144.4 \text{ kN}$ (CV = 3.4%)

The corresponding values of each group can also be found in Table 1. All perpendicular to the grain embedded rods failed in withdrawal (see Figure 8) with an average capacity $F_{ax,90^\circ}$ of 155 kN. This is higher than the original estimation of $F_{ax,est} = 120 \text{ kN}$ which was used to define the service-level cyclic loading up to 40 %. As it can be seen in Figure 8, all individual tests of the reinstalled rods are well within the mean curves. Consequently, the reinstallation of the perpendicular to the grain embedded rods (group 2) showed no effect on the withdrawal capacity. An example of withdrawal failure of the perpendicular to the grain embedded rod is shown in Figure 10.

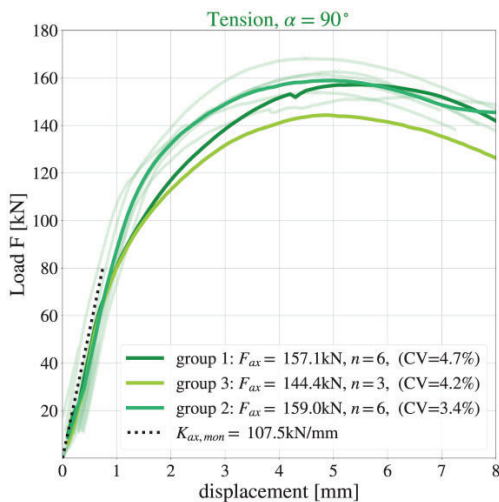


Figure 8: Capacity $F_{ax,90^\circ}$ of perpendicular to the grain embedded rods in withdrawal failure

For the rods inserted parallel to the grain, both splitting (s) and withdrawal (w) failures were observed. Examples of both failure modes are shown in Figure 11. The average capacity was 123.8 kN for splitting and 116.9 kN in case of withdrawal over all groups as illustrated in the load displacement curves of Figure 9. Again the individual measurements of group 2 are plotted in the background in a fainter colour. The capacity $F_{ax,0^\circ}$ of the reinstalled rods in group 2 was approximately 20 % lower in withdrawal and 10 % lower in splitting than the reference group 3 and group 1. However this decrease can partly be explained by one outlier, that failed in withdrawal at a very low capacity of 90 kN. It is therefore questionable, if the lower capacity can be related to the effect of the reinstallation, or if it lays within the natural variability in test results. The parallel to the grain embedded rods cover generally a bigger range in individual test results for all investigated parameters. This is because, in contrary to the perpendicular to the grain embedded ones, only one lamella of the glulam is penetrated and no homogenization effect is created.

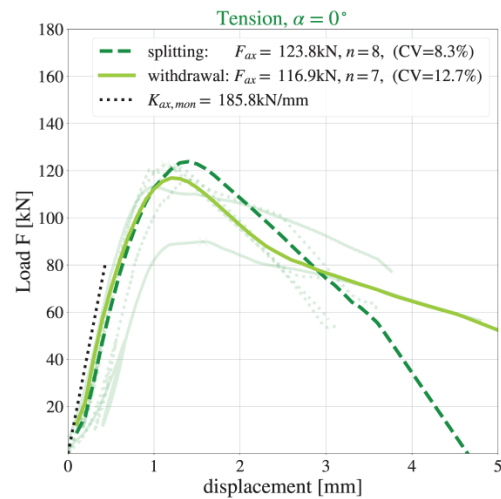


Figure 9: Capacity $F_{ax,0^\circ}$ of parallel to the grain embedded rods for splitting (s) and withdrawal (w) failure

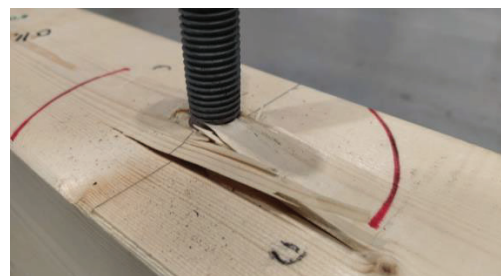


Figure 10: Failure mode of perpendicular to the grain embedded rods in withdrawal

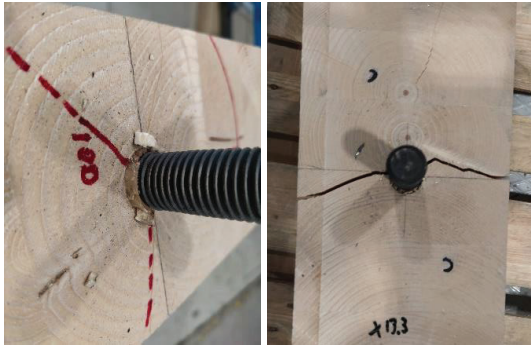


Figure 11: Failure modes of parallel to the grain embedded rods in withdrawal (left) and splitting (right)

5 – CONCLUSION

The outcomes of this study suggest that screwed-in threaded rods have a good potential for reuse. They allow easy and fast assembly and disassembly and feature high stiffness and capacity even after reassembly. The most important results regarding the mechanical properties after reinstallation are as follows:

- No significant effect of the reinstallation of the perpendicular to the grain embedded rods on the capacity could be measured. The capacity of the parallel embedded rods was slightly lower after reassembly, which may be attributed to reassembly or the natural variability of the material.
- A decrease in monotonic axial stiffness after reinstallation was observed in all specimens. The remaining stiffness after reassembly was 73 % for the rods embedded perpendicular to the grain and 80 % for the rods embedded parallel to the grain.
- The monotonic stiffness in compression loading is lower than in tension. The reinstallation process seems to have a smaller effect on the axial stiffness in compression loading than in tension.
- The cyclic axial stiffness in tension or compression was generally less effected by the reassembly than the monotonic axial stiffness. However, under fully reversed loading, the effect of the reassembly was most prominent due to increased pinching after the second assembly. The remaining stiffness was 61 % for rods embedded perpendicular to the grain and 78 % for rods embedded parallel to the grain. This finding is due to greater pinching effect for reassembled perpendicular to grain rods.

This pilot study gave some insights on alternated mechanical properties of threaded rods after reinstallation. However, further testing is recommended to draw more accurate conclusions. Further investigations could explore different load sequences, climate histories and angles to the grain to better reflect realistic scenarios. Additionally, testing a larger number of specimens would improve the reliability of the findings.

6 – ACKNOWLEDGEMENTS

This work has been carried out within the LifeLine-2050 project, funded by the Faculty of Engineering (IV) at the Norwegian University of Science and Technology (NTNU). The LifeLine-2050 project is a flagship project with the NTNU's Centre for Green Shift in the Built Environment (Green2050). The authors gratefully acknowledge the support of Green2050's partners and the encouragement of the innovation committee of IV faculty at NTNU. Moreover, the authors would like to thank Ingeborg Sennesvik Sund and Isa Ghorbani for their assistance with the lab work as part of their master's theses.

6 – REFERENCES

- [1] P. Hradil, A. Talja, M. Wahlström, S. Huuhka, J. Lahdensivu, and J. Pikkuvirta, *Re-use of structural elements; Environmentally efficient recovery of building components*. 2014. doi: 10.13140/2.1.1771.9363.
- [2] L.-M. Ottenhaus, Z. Yan, R. Brandner, P. Leardini, G. Fink, and R. Jockwer, "Design for adaptability, disassembly and reuse – A review of reversible timber connection systems," *Construction and Building Materials*, vol. 400, p. 132823, Oct. 2023, doi: 10.1016/j.conbuildmat.2023.132823.
- [3] C. Binck and A. Frangi, "On stiffness and strength of glued-in rods and threaded rods parallel to the grain," 2024.
- [4] O. A. Hegeir and H. Stamatopoulos, "Experimental investigation on axially-loaded threaded rods inserted perpendicular to grain into cross laminated timber," *Construction and Building Materials*, vol. 408, p. 133740, Dec. 2023, doi: 10.1016/j.conbuildmat.2023.133740.
- [5] H. Stamatopoulos and K. A. Malo, "On strength and stiffness of screwed-in threaded rods embedded in softwood," vol. 261, p. 119999, Nov. 2020, doi: 10.1016/j.conbuildmat.2020.119999.
- [6] H. Stamatopoulos and K. A. Malo, "Withdrawal stiffness of threaded rods embedded in timber

- elements,” vol. 116, pp. 263–272, Jul. 2016, doi: 10.1016/j.conbuildmat.2016.04.144.
- [7] H. Stamatopoulos and K. A. Malo, “Withdrawal capacity of threaded rods embedded in timber elements,” vol. 94, pp. 387–397, Sep. 2015, doi: 10.1016/j.conbuildmat.2015.07.067.
- [8] O. A. Hegeir, K. A. Malo, and H. Stamatopoulos, “An innovative slip-friction moment-resisting connection using screwed-in threaded rods in cross laminated timber and steel coupling parts: An experimental study,” *Engineering Structures*, vol. 318, p. 118654, Nov. 2024, doi: 10.1016/j.engstruct.2024.118654.
- [9] *EN 14080:2013, Timber structures - Glued laminated timber and glued solid timber - Requirements*, Brussels, Belgium., 2013.
- [10] *EN 1995-1-1:2004+AC:2006+A1:2008D, Design of timber structures-Part 1-1: General- Common rules and rules for buildings*, Brüssels, Belgium., 2008.
- [11] *EN 26891:1991, timber structures; joints made with mechanical fasteners; general principles for the determination of strength and deformation characteristics (ISO 6891:1983)*, Brüssels, Belgium., 1991.
- [12] *EN 12512:2001+A1:2005, Cyclic testing of joints made with mechanical fasteners*, Brussels, Belgium., 2005.